УДК 539.172

THREE-PARTICLE STRUCTURE OF THE HALO NUCLEUS ^{6}Li

B. E. Grinyuk, I. V. Simenog

Bogolyubov Institute for Theoretical Physics, National Academy of Sciences of Ukraine, Kyiv

The three-particle model for ^{6}Li nucleus (α-cluster, and two halo nucleons p and n) is used to study the structure properties of this system within the variational method with Gaussian basis. The ground triplet ($J^\pi = 1^+$) and the excited singlet ($J^\pi = 0^+$) states of ^{6}Li are studied. For this purpose, potentials of the np- and $N\alpha$-interaction are proposed to give description of the elastic S-phases at low energies simultaneously with correct values of the binding energy and the charge radius of ^{6}Li nucleus. The density distributions, elastic form factors, pair correlation functions, clusterization coefficients, and momentum distributions of ^{6}Li nucleus are studied.

Introduction

A number of approaches are known (see reviews [1 - 3]) to treat the structure of the halo nucleus ^{6}Li within the three-particle model (α-particle plus two nucleons). They are competitive with the approaches [4, 5] (see also the earlier study [6]) starting from the six-nucleon system. Moreover, the three-particle model can be of even a higher accuracy than commonly assumed (see the results for ^{6}He nucleus [7]), if the $N\alpha$-interaction potentials are chosen to reproduce the energy and radius of the nucleus in addition to the $N\alpha$-phase shifts. In the present paper, the preliminary results reported in [8] are developed. In addition to the structure of the ground triplet ($J^\pi = 1^+$) state of ^{6}Li nucleus, we study the ^{6}Li singlet ($J^\pi = 0^+$) state and supplement the study of the main structure functions with the analysis of the cluster coefficients. To calculate the parameters of the bound states with high precision, we use the variational method in the Gaussian representation with optimization of the bases [9, 10].

A model of $N\alpha$-interaction for the three-particle Hamiltonian

The three-particle model of halo nuclei ^{6}Li and ^{6}He deals with different versions of the $N\alpha$-interaction [1 - 2] constructed to reproduce the $N\alpha$-phase shifts at low-energies. We propose simple $N\alpha$-interaction potentials to fit simultaneously the S-phase shifts, energy, and rms radius of the nucleus under consideration. Such a potential contains a local attractive potential and a non-local (separable) repulsive one of rather large intensity g to simulate the Pauli principle:

$$\hat{V}_{N\alpha}\Psi(r) = V(r)\ \Psi(r) + g u(r) \int u(r_1)\ \Psi(r_1)\ d\mathbf{r}_1. \quad (1)$$

This construction generalizes the well-known potentials with forbidden states [11, 2] to the case of finite intensities of the repulsion, g, and an arbitrary $u(r)$ which is not identical to the forbidden state wave function though appears to be close to it [7].

To study the ground triplet ($J^\pi=1^+$) state of ^{6}Li, we consider the three-particle Hamiltonian

$$\hat{H} = \frac{\mathbf{p}_1^2}{2m_p} + \frac{\mathbf{p}_2^2}{2m_n} + \frac{\mathbf{p}_3^2}{2m_\alpha} + V_{np}(r_{12}) + $$

$$+\hat{V}_{p\alpha}(r_{13}) + \hat{V}_{n\alpha}(r_{23}) + V_{Coul}(r_{13}) \quad (2)$$

with the interaction potential $V_{np}(r_{12})$ in the triplet state between the halo neutron and proton, with $\hat{V}_{N\alpha}$ of the type (1), and with the Coulomb interaction potential between the proton and α-particle. In the case of the singlet ($J^\pi = 0^+$) state of ^{6}Li, we have the interaction $V_{np}(r_{12})$ between the halo nucleons in the singlet state. For the ground state ($J^\pi = 0^+$) of ^{6}He nucleus, the Coulomb interaction is absent, and the neutron-neutron interaction $V_{nn}(r_{12})$ is taken in the singlet state. Thus, all the three states mentioned above correspond (within the three-particle model) to different three-particle Hamiltonians. The energy levels of these states are below the corresponding breakup thresholds.

The results obtained for the main structure characteristics of ^{6}Li and ^{6}He nuclei can be of a rather high accuracy even for the simplest variants of interaction potentials [7], if these potentials reproduce the low-energy phase shifts parameters simultaneously with the energy and the rms radii of the nuclei. One can use realistic V_{NN} potentials (as in ref. [1, 2]) or semi-realistic ones fitted to describe simultaneousely the properties of three- and four-nucleon nuclei [10]. But the main results for the halo nucleus ^{6}Li we obtain here with the singlet and triplet V_{np} interaction potentials in a rather simple form (Table 1). These potentials reproduce the corresponding phase shifts (up to ~300 MeV) together with their low-energy parameters in a quite reasonable way. The triplet V_{np} potential reproduces,

in addition to the triplet phase shift and its low-energy parameters $a_{np,t}$ and $r_{0\,np,t}$, also the deuteron binding energy ε_d and the deuteron charge radius R_d (Table 1). The radius R_d is calculated with regard for the proton radius $r_p = 0.875$ fm [12].

Table 1. **Parameters of the singlet and triplet V_{np} potentials (energies in MeV, radii in fm)**

Potential $V_{np}(r)$ in the singlet state:	$a_{np,s}$	$r_{0\,np,s}$	Potential $V_{np}(r)$ in the triplet state:	$a_{np,t}$	$r_{0np,t}$	ε_d	R_d
$V_{np}(r)=\sum_{k=1}^{3}V_{0k}\exp\left(-(r/r_{0k})^2\right)$ $V_{01}=455.265$, $r_{01}=0.647$, $V_{02}=-168.26$, $r_{02}=0.946$, $V_{03}=-28.24$, $r_{03}=1.792$	-23.749	2.809	$V_{np}(r)=\sum_{k=1}^{2}V_{0k}\exp\left(-(r/r_{0k})^2\right)$ $V_{01}=840.545$, $r_{01}=0.440$, $V_{02}=-146.046$, $r_{02}=1.271$	5.424	1.783	2.224576	2.140
Experiment	-23.749± ±0.008	2.81± ±0.05	Experiment	5.424± ±0.003	1.760± ±0.005	2.224575(9)	2.1402± ±0.0028

It should be noted that any reasonable variations of the form of local central *NN*-potentials at fixed low-energy scattering parameters do not change essentially the results for ^{6}Li and ^{6}He nuclei within the three-particle model. This can be explained mainly by a short range of nuclear forces in comparison with the distances between halo nucleons. The absolutely another situation takes place for *Nα*-potentials of the type (1), and one has to choose the parameters of the potentials by fitting the *Nα*-phase shifts at low energies simultaneously with the energies and radii of the nuclei [7].

Phase shifts for potentials of the general type (local and non-local terms), with the Coulomb interaction involved

For local potentials, the calculation of phase shifts within the variable phase approach is known to be a rather simple procedure [13, 14]. But, in the case of non-local potentials of the general type $\hat{V}(\mathbf{r},\mathbf{r}')$, there exists an essential difficulty. We recall that the equation for the phase shift within the variable phase approach [13] may contain singularities of the exponential argument if $ks+\delta(s)=\pi n$. The main difficulty is that the position of the poles in the equation is unknown *a priori*, i.e. before the solution $\delta(s)$ is found. At the same time, the solution itself has no singularities, i.e. the singularities in the equation have no physical sense.

In [7], it is shown how to overcome this difficulty in the case of short-range potentials of the type (1): instead of the nonlinear equation of the variable phase approach [13], we deal with a system of two linear equations without singularities. Consider now a more general case with the Coulomb repulsion involved. The solution $u_l(r)$ of the Schrödinger equation (for an arbitrary partial wave)

$$u_l''(r)+\left(k^2-\frac{l(l+1)}{r^2}-\frac{\frac{2\mu}{\hbar^2}Z_1Z_2e^2}{r}\right)u_l(r)-$$

$$-\int_0^\infty V_l(r,r_1)\,u_l(r_1)\,dr_1=0, \qquad (3)$$

where

$$V_l(r,r_1)=2\pi rr_1\int_0^\pi V(\mathbf{r},\mathbf{r}_1)P_l(\cos\theta)\sin\theta\,d\theta, \qquad (4)$$

can be presented in the form

$$u_l(r)=C_1(r)F_l(kr,\eta)+C_2(r)\,G_l(kr,\eta). \qquad (5)$$

Here, $F_l(kr,\eta)$ and $G_l(kr,\eta)$ are the regular and irregular Coulomb functions, respectively, $\eta\equiv\dfrac{\mu Z_1Z_2e^2}{\hbar^2k}$ is the Coulomb parameter, μ is the reduced mass of the two scattering particles with Z_1e and Z_2e charges. The functions $C_1(r)$ and $C_2(r)$ can be shown to obey the system of equations

$$\begin{cases} C_1'(r)=\dfrac{G_l(kr,\eta)}{k}\displaystyle\int_0^\infty V_l(r,r_1)\,\left(C_1(r_1)F_l(kr_1,\eta)+C_2(r_1)\,G_l(kr_1,\eta)\right)dr_1, \\ C_2'(r)=-\dfrac{F_l(kr,\eta)}{k}\displaystyle\int_0^\infty V_l(r,r_1)\,\left(C_1(r_1)F_l(kr_1,\eta)+C_2(r_1)\,G_l(kr_1,\eta)\right)dr_1 \end{cases} \qquad (6)$$

with the boundary conditions $C_1(0) \neq 0$ (in particular, $C_1(0) = 1$) and $C_2(0) = 0$. Then the phase shift $\gamma_l(k)$ (which is a part of the total phase shift $\delta_l = \gamma_l + \beta_l$, where β_l is the well-known purely Coulomb phase shift) can be found from the relation

$$tg\left(\gamma_l(k)\right) = \lim_{r\to\infty} \frac{C_2(r)}{C_1(r)}. \qquad (7)$$

The low-energy parameters of this phase shift can be derived from the expansion [14] (e.g., for $l = 0$)

$$\frac{2\pi\eta}{\exp(2\pi\eta)-1} k\ ctg\left(\gamma_0(k)\right) + 2k\eta\ h(\eta) = -\frac{1}{a_p} + \frac{1}{2} r_{0p} k^2 - P_p r_{0p}^3 k^4 + \ldots, \qquad (8)$$

where $h(\eta) \equiv \eta^2 \sum_{n=1}^{\infty} \frac{1}{n(n^2+\eta^2)} - \ln(\eta) - \gamma$, and $\gamma = 0.5772...$ is the Euler constant. The low-energy parameters can be also found from the corresponding limiting equations. For example, to calculate the nuclear-Coulomb scattering length a_p ($l = 0$), we introduce

$$\tilde{C}_1(r) \equiv C_1(r) \frac{2\pi\eta}{\exp(2\pi\eta)-1},$$

$$\tilde{C}_2(r) \equiv \lim_{k\to 0} \frac{C_2(r)}{k}. \qquad (9)$$

Then in the limit $k \to 0$, equations (6) yield the system of equations

$$\begin{cases} \tilde{C}_1'(r) = H_1\left(\frac{r}{R}\right) \int_0^\infty V_0(r, r_1) \left(\tilde{C}_1(r_1)\ r_1 L_1\left(\frac{r_1}{R}\right) + \tilde{C}_2(r_1)\ H_1\left(\frac{r_1}{R}\right)\right) dr_1, \\ \tilde{C}_2'(r) = -r\ L_1\left(\frac{r}{R}\right) \int_0^\infty V_0(r, r_1) \left(\tilde{C}_1(r_1)\ r_1 L_1\left(\frac{r_1}{R}\right) + \tilde{C}_2(r_1)\ H_1\left(\frac{r_1}{R}\right)\right) dr_1 \end{cases} \qquad (10)$$

with the initial conditions $\tilde{C}_1(0) \neq 0$ (in particular, $\tilde{C}_1(0) = 1$) and $\tilde{C}_2(0) = 0$. In Eqs. (10), $L_1(x) \equiv \frac{1}{\sqrt{x}} I_1\left(2\sqrt{x}\right)$, $H_1(x) \equiv 2\sqrt{x} K_1\left(2\sqrt{x}\right)$, where I_1 and K_1 are the modified Bessel functions, and the parameter $\frac{1}{R} \equiv \frac{2\mu Z_1 Z_2 e^2}{\hbar^2}$. The nuclear-Coulomb scattering length is obtained as

$$a_p = -\lim_{r\to\infty} \frac{\tilde{C}_2(r)}{\tilde{C}_1(r)}. \qquad (11)$$

In the case of a potential of the type (1), the separable part of the interaction reveals itself only in the partial wave with $l = 0$. Thus, the phase shifts and their low-energy parameters for the rest orbital states can be calculated within the known standard procedures [13, 14].

Three-body problem within variational approach with Gaussian basis, and parameters of the *Nα*-potentials

We choose the parameters of *Nα*-potentials of the type (1) in such a way that to reproduce the phase shifts of the *Nα*-scattering at low energies simultaneously with the energy and charge radius of a nucleus under consideration. Calculations of the energies and the wave functions are carried out with enough precision using the known variational method with Gaussian bases [15, 16]. We also take advantage of the optimization schemes [9, 10] to minimize the dimension of the basis due to special variational procedures for nonlinear parameters. It appears to be sufficient to take 100÷150 components of the Gaussian basis to achieve a necessary high accuracy.

Consider the ^{6}Li ground state ($J^\pi = 1^+$). If we want to keep a simple model for the potential $\hat{V}_{p\alpha}$ (the same as for $\hat{V}_{n\alpha}$ [7], with one Gaussian function for the attractive part and the one for $u(r)$), the charge independence of nuclear forces $\hat{V}_{p\alpha} = \hat{V}_{n\alpha}$, and a simple form for the potentials $\hat{V}_{pn}$ (see Table 1) and $\hat{V}_{nn}$ (see ref. [7]), we are faced with the following difficulty. The number of parameters of the potential $\hat{V}_{p\alpha}$ or $\hat{V}_{n\alpha}$ is only four, and it is impossible to fit simultaneously the energies and radii of both nuclei ^{6}He and ^{6}Li in addition to the *nα*- and *pα*-phase shifts. For example, the calculated energy of ^{6}Li appears to be ≈ -4.98 MeV (instead of the experimental value -3.70 MeV) in the case $\hat{V}_{p\alpha} = \hat{V}_{n\alpha}$ with the parameters used for ^{6}He [7]. In the present paper, we consider two following

possibilities to keep the potentials $\hat{V}_{p\alpha}$ and $\hat{V}_{n\alpha}$ in the simplest form. The first one (further denoted as (***I***)) is to break the charge symmetry ($\hat{V}_{p\alpha} \neq \hat{V}_{n\alpha}$) and to take $\hat{V}_{p\alpha}$ and $\hat{V}_{n\alpha}$ with somewhat different parameters. The *nα*- and *pα*-phase shifts are fitted independently. Due to the additional independent parameters at our disposal, we can reproduce the experimental values of the energies and radii for both nuclei (for ^{6}Li, Table 2). The second possibility (denoted as (***II***)) is to save the charge symmetry $\hat{V}_{p\alpha} = \hat{V}_{n\alpha}$, but to adjust new parameters of the *Nα*-potential to fit the experimental values for ^{6}Li alone. One version of such a potential is given in Table 2 as well. The third possibility with a more complicated form of potentials (including the account of the tensor forces in the *NN*-interaction, and the *l*-dependence of *Nα*-potentials) needs the separate consideration.

Table 2. **Parameters of the $\hat{V}_{p\alpha}$ potentials used in the calculations of the ^{6}Li ground state and the calculated radii of this nucleus (energies in MeV, radii in fm)**

$\hat{V}_{p\alpha}$ potential	$E_{^6Li}$	R_{ch}	R_m	r_{np}	$r_{n\alpha}$	$r_{p\alpha}$	R_n	R_p	R_α
(***I***), $V_{p\alpha} \neq V_{n\alpha}$ ($V_{n\alpha}$ see [7]) $V_0(r) = -43.11\exp\left(-(r/2.34)^2\right)$ $g = 135.0$ MeV fm^{-3}, $u(r) = \pi^{-3/4}\exp\left(-(r/2.67)^2\right)$	-3.699	2.560	2.553	3.187	4.203	4.314	3.020	3.123	1.323
(***II***), $V_{p\alpha} = V_{n\alpha}$ $V_0(r) = -45.13\exp\left(-(r/2.37)^2\right)$ $g = 140.0$ MeV fm^{-3}, $u(r) = \pi^{-3/4}\exp\left(-(r/2.7)^2\right)$	-3.699	2.560	2.568	3.193	4.281	4.313	3.081	3.112	1.337
Experiment	-3.699± ±0.001 [17]	2.56± ±0.05 [18]	2.45± ±0.07 [19]						

For the potentials from Table 2, the *pα*-phase shifts in the $S_{1/2}$ state are in a reasonable agreement with the experimental phase shift at low energies up to the breakup threshold (~22 MeV). In both cases, we have fitted the energy and the rms charge radius of ^{6}Li nucleus. We recall that the binding energy of ^{6}Li is greater than that of ^{6}He mainly due to the fact that the triplet potential V_{np} is somewhat more attractive than the singlet potential V_{nn} (in spite of the presence of additional Coulomb repulsion in ^{6}Li). At the same time, the charge radius of ^{6}Li is greater than that of ^{6}He mainly due to the presence of one proton in the halo of ^{6}Li. It follows from the calculations that the matter radius R_m of ^{6}Li (see Table 2) appears to be almost the same as that of ^{6}He [7] and somewhat greater than the experimental value $R_m\left(^6\mathrm{Li}\right) = 2.45 \pm 0.07$ fm [19].

Table 3. **Parameters of the $\hat{V}_{p\alpha}$ potential used in the calculations for ^{6}Li singlet ($J^\pi = 0^+$) state, and the calculated radii of this state (energies in MeV, radii in fm)**

$\hat{V}_{p\alpha}$ potential	$E_{^6Li}(J^\pi = 0^+)$	R_{ch}	R_m	r_{np}	$r_{n\alpha}$	$r_{p\alpha}$	R_n	R_p	R_α
$V_0(r) = -50.208\exp\left(-(r/2.342)^2\right)$ $g = 135.0$ MeV fm^{-3}, $u(r) = \pi^{-3/4}\exp\left(-(r/2.7)^2\right)$	- 0.13	2.813	2.803	4.663	4.704	4.824	3.562	3.668	1.392
Experiment	-0.13								

Consider now ^{6}Li nucleus in the loosely bound singlet state ($J^\pi = 0^+$) with an energy of about -0.13 MeV. To have the concordant results simultaneously for all the three states (i.e. ^{6}He and ^{6}Li in the ground state, and ^{6}Li in the singlet state) is, all the more, impossible for simple models of potentials. We slightly adjust the parameters of the potential $V_{p\alpha}$ to obtain the experimental value of the

^{6}Li singlet state energy (with the use of the singlet potential V_{np} for the halo nucleons in the form presented in Table 1). In Table 3, the parameters of one version of such a potential $V_{p\alpha}$ are given. The corresponding phase shift in the $S_{1/2}$ state is close to the experimental data below the breakup threshold. The potential $V_{n\alpha}$ used together with $V_{p\alpha}$ is the same as that proposed to study ^{6}He nucleus [7]. The obtained rms radius R_{ch} (see Table 3) can only predict the order of magnitude for this parameter, because, as mentioned above, by varying the potentials $V_{p\alpha}$ and $V_{n\alpha}$, one can reproduce any radius within a wide range of its values at the fixed experimental energy of ^{6}Li in this state and the fixed $N\alpha$-phase shift at low energies. The rest rms radii are correlated with R_{ch}.

Wave function, density distributions and form factor of ^{6}Li nucleus

The properties of the structure functions of ^{6}Li and ^{6}He nuclei become more understandable if one considers their wave functions. In particular, the wave function squared, averaged over the angles, and multiplied by the factor $r^2\rho^2$,

$$P(r,\rho) = r^2\rho^2 \int d\Omega \left|\Phi(\mathbf{r},\boldsymbol{\rho})\right|^2, \qquad (12)$$

is known to have two peaks (Fig. 1) corresponding to configurations of the so-called "cigar" (where the halo nucleons are at the opposite sides, and the α-particle is at the center) and "triangle" (where two coupled nucleons of the halo and the α-particle move around the center of mass of ^{6}Li). Since a free dineutron does not exist in a bound state, while the deuteron does exist, the configuration of a "triangle" is more pronounced in ^{6}Li nucleus than in ^{6}He. The wave function of the singlet state of ^{6}Li has a structure more close to that of ^{6}He than to that of the ^{6}Li ground state (see Fig. 1, *c*), but the radii of the singlet state of ^{6}Li are greater (compare the Tables 2 and 3, and the results for ^{6}He [7]) mainly due to the Coulomb repulsion and some difference in nuclear potentials.

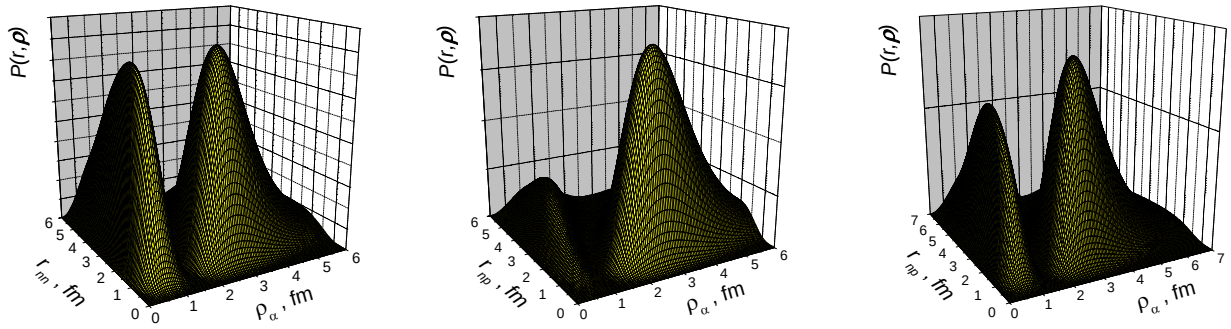

a *b* *c*

Fig. 1. Probability density $P(r,\rho)$ (12) for ^{6}He (*a*) and ^{6}Li (*b*) nuclei in the ground state, and (*c*) – the same for ^{6}Li in the singlet state.

Here and further, we give the results for structure functions obtained with potential (***II***) from Table 2. Almost the same results are obtained with potential (***I***).

The density distribution $\rho_j(r)$ of the point-like particle *j* with respect to the center of mass of the system with the wave function $|\Phi\rangle$ is known to be

$$\rho_j(r) = \langle\Phi|\ \delta\left(\mathbf{r} - \left(\mathbf{r}_j - \mathbf{R}_{c.m.}\right)\right)\ |\Phi\rangle. \qquad (13)$$

In Fig. 2, the density distributions of the "point-like" neutron and proton of the halo of ^{6}Li, and the distribution of neutrons in the halo of ^{6}He are presented (see Fig. 2, *a*), as well as the α-particle center-of-mass density distribution (see Fig. 2, *b*) is shown. A pronounced "halo" in the distribution of the α-particle center-of-mass is seen for both nuclei, and this structure is explained by the presence of two different configurations in the total wave function. For the singlet state of ^{6}Li nucleus, the same dependences look very similar to those for the ^{6}Li ground state, but they have somewhat greater radii due to the fact that the energy of ^{6}Li nucleus in the singlet state is more close to the $^6\text{Li} \rightarrow \alpha + p + n$ threshold (≈0.13 MeV) than the energy of the ground state of ^{6}Li to the $^6\text{Li} \rightarrow \alpha + d$ threshold (≈1.47 MeV). The both binding energies are close to zero in comparison with the average kinetic or potential energy of the system (each of them is about 25 - 30 MeV).

To determine the total charge distributions of ^{6}Li and ^{6}He with regard for the charge distribution of the α-particle itself and that of the proton (for ^{6}Li), one has to calculate

$$\rho_{ch,\,^6Li}(r) = \frac{2}{3}\int \rho_{\alpha\ c.m.}(\mathbf{r}-\mathbf{r}')\ n_{ch,\,^4He}(r')d\mathbf{r}' +$$

$$+\frac{1}{3}\int \rho_p(\mathbf{r}-\mathbf{r}')\ n_{ch,p}(r')d\mathbf{r}',$$

$$\rho_{ch,\,^6He}(r) = \int \rho_{\alpha\ c.m.}(\mathbf{r}-\mathbf{r}')\, n_{ch,\,^4He}(r')d\mathbf{r}', \qquad (14)$$

where $n_{ch,\,^4He}(r)$ and $n_{ch,\,p}(r)$ are the charge density distributions of ^{4}He and of the proton, respectively. In Fig. 3, the calculated charge density distributions (normalized to unity) for ^{6}Li and ^{6}He nuclei are compared with that for ^{4}He. After the integrations in (14), the calculated charge distributions appear to be smooth functions. If the normalization of $\rho_{ch}(r)$ for ^{6}Li and ^{6}He nuclei were chosen proportional to Z, then both densities would be close at $r = 0$.

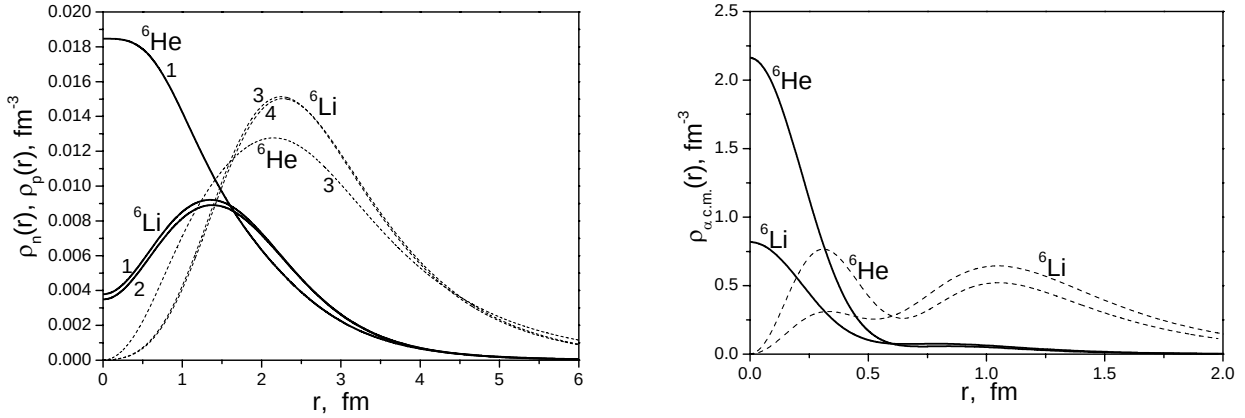

a *b*

Fig. 2. Density distributions of the halo neutron (curves *1*) and proton (curve *2*) in ^{6}Li and ^{6}He nuclei. The dashed lines show $r^2\rho(r)\cdot 0.5$ for the neutron (curves *3*) and proton (curve *4*) (*a*). Distributions of the α-particle in the same nuclei. The dashed lines depict $r^2\rho_{\alpha\ c.m.}(r)\cdot 10$ (*b*).

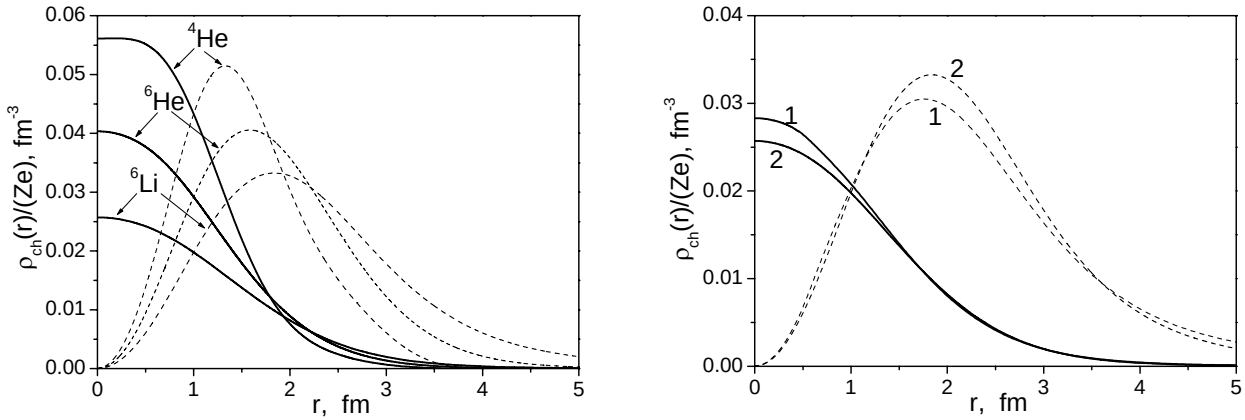

a *b*

Fig. 3. Charge density distributions for ^{6}He and ^{6}Li (the curve for ^{4}He – experimental data) (*a*). Charge density distribution for the singlet state of ^{6}Li (solid curve *1*) compared with that of the ground state of ^{6}Li (solid curve *2*) (*b*). In the figures, the dashed lines depict $r^2\rho_{ch}(r)$.

The rms radii of the ^{6}Li nucleus are listed in Tables 2 and 3. They can be compared with the corresponding radii of ^{6}He [7]. Due to the motion of the *α*-particle around the center of mass of the system in ^{6}Li and ^{6}He nuclei and also due to the presence of a proton in the ^{6}Li halo, the charge rms radii obey the inequality $R_{ch,^6Li} > R_{ch,^6He} > R_{ch,^4He}$. Tables 2 and 3 contain also the rms radii R_j for the "point-like" particles of the halo and of the *α*-particle center-of-mass distribution. We also calculate the rms relative distances r_{ij}:

$$r_{ij} = \left(\int r^2 g_{ij}(r)\, d\mathbf{r}\right)^{\frac{1}{2}}, \qquad (15)$$

where $g_{ij}(r)$ are the pair correlation functions (see below). The values of R_j and r_{ij} are interrelated as follows:

$$r_{ij}^2 = \left(1+\frac{m_i}{m_j}\right)R_i^2 + \left(1+\frac{m_j}{m_i}\right)R_j^2 - \frac{m_k^2}{m_i m_j}R_k^2, \qquad (16)$$

where *i*, *j*, and *k* are the numbers of different particles of the three-particle system. We calculated

R_j and r_{ij} independently and verified the obtained results by using (16).

The form factors corresponding to the charge density distributions (14) are known to be

$$F_{ch,\,^6He}\left(q^2\right)=F_{\alpha\ c.m.}\left(q^2\right)\cdot F_{ch,\,^4He}\left(q^2\right),$$
$$F_{ch,\,^6Li}\left(q^2\right)=\frac{2}{3}F_{\alpha\ c.m.}\left(q^2\right)\cdot F_{ch,\,^4He}\left(q^2\right)+\frac{1}{3}F_p\left(q^2\right)\cdot f_{ch,p}\left(q^2\right), \quad (17)$$

where $F_{\alpha\ c.m.}\left(q^2\right)$ and $F_p\left(q^2\right)$ are the form factors obtained within the three-particle model with the "point-like" particles, while $F_{ch,\,^4He}\left(q^2\right)$ is the experimental charge form factor of ^{4}He, and $f_{ch,p}\left(q^2\right)$ is that of the proton. In Fig. 4, the charge form factors (17) are shown and compared with the experimental data for ^{4}He and ^{6}Li. The position of $q^2_{\min}$ in the case of the ^{6}He form factor is explained mainly by the behavior of the ^{4}He form factor. Due to a slowly decreasing $F_{\alpha\ c.m.}\left(q^2\right)$ (see Fig. 4, the upper curve α), relation (17) yields the inequality $\left|F_{ch,\,^6He}\left(q^2\right)\right|<\left|F_{ch,\,^4He}\left(q^2\right)\right|$. In the case of ^{6}Li nucleus, the form factor $F_p\left(q^2\right)$ (see Fig. 4, *b*, the curve *p*) of the "point-like" proton distribution plays its role as well. Since the behavior of the form factors at small q^2 is determined by the value of R_{ch}, and our potentials are fitted to reproduce the experimental charge radii, the coincidence of the calculated form factors with the experimental data at small q^2 is good in all the cases.

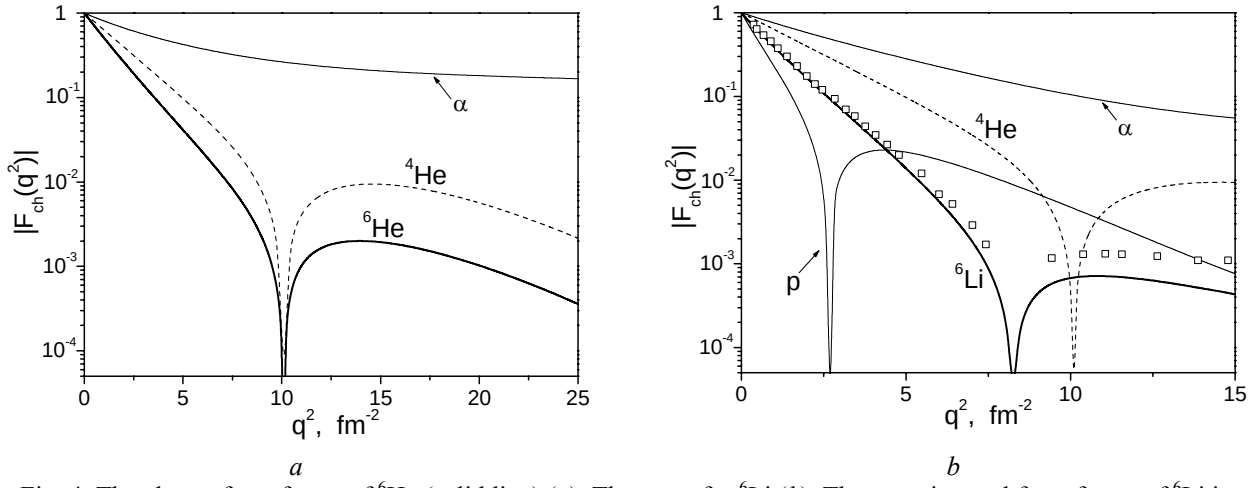

Fig. 4. The charge form factor of ^{6}He (solid line) (*a*). The same for ^{6}Li (*b*). The experimental form factor of ^{6}Li is shown by squares, and the dashed lines depict the experimental form factor of ^{4}He.

Pair correlation functions, coefficients of clusterization, and momentum distributions

Consider the pair correlation functions

$$g_{ij}\left(r\right)=\left\langle\Phi\left|\delta\left(\mathbf{r}-\left(\mathbf{r}_i-\mathbf{r}_j\right)\right)\right|\Phi\right\rangle. \quad (18)$$

The function $g_{ij}\left(r\right)$ is the probability density to find the pair of particles *i* and *j* at a distance *r* inside the system under consideration. For the pairwise local potentials, the average potential energy is directly expressed in terms of the integrals over the potentials multiplied by the corresponding correlation functions. These functions are also used below to estimate the probability for two-particle clusters to exist in ^{6}Li and ^{6}He nuclei.

In Fig. 5, we present the pair correlation functions for ^{6}Li nucleus. The function $g_{np}\left(r\right)$ for ^{6}Li (similar to $g_{nn}\left(r\right)$ for ^{6}He [7]) demonstrates an essential decrease at short distances, which is explained by the presence of a short-range repulsion in the interaction potential V_{np}.

Consider the amplitude [20]

$$f_{^6Li,\,d}\left(\rho\right)=\int\varphi_d^*\left(r_{np}\right)\,\Phi_{^6Li}\left(\mathbf{r}_{np},\boldsymbol{\rho}\right)\,d\mathbf{r}_{np}, \quad (19)$$

which depends on the distance ρ of the α-particle from the center of mass of ^{6}Li (the same function is denoted by $I\left(\rho\right)$ in ref. [21]). In (19), $\varphi_d\left(r_{np}\right)$ denotes the deuteron wave function. The quantity $\left|f_{^6Li,\,d}\left(\rho\right)\right|^2$ (Fig. 6, *a*, curve *1*) is the value reflecting the probability density "to find the deuteron" at a definite distance ρ from the α-particle. There are two peaks in the $\rho^2\left|f_{^6Li,\,d}\left(\rho\right)\right|^2$ profiles (see Fig. 6, *a*,

curve *5*), which correspond to the configurations of "cigar" (short distances) and "triangle" (at ~3÷4 fm). The coefficient of clusterization

$$C_d^{(^6Li)} = \int \left| f_{^6Li,\,d}(\rho) \right|^2 d\boldsymbol{\rho} \qquad (20)$$

allows one to estimate the probability "to find a deuteron" in ^{6}Li nucleus. It appears to be 0.70 (about 0.09 is the contribution of the "cigar", and about 0.61 is that of the "triangle"). We note that, in the case of a bound system of three identical particles at the extremely large coupling constant [20], the corresponding clusterization coefficient approaches $(3/2)^{3/4}\left(2/\left(1+\sqrt{3/2}\right)\right)^3 \approx 0.9847$, whereas this coefficient approaches zero as the coupling constant decreases to the two-particle critical value.

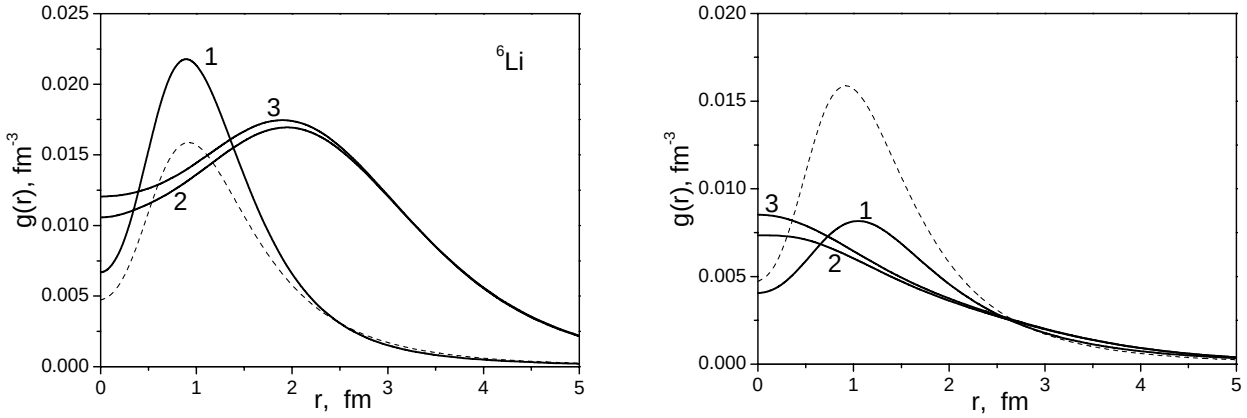

a *b*

Fig. 5. Pair correlation functions for ^{6}Li in the ground state (*1* - $g_{np}(r)$; *2* - $g_{p\alpha}(r)\cdot 5$; *3* - $g_{n\alpha}(r)\cdot 5$) (*a*). The same for ^{6}Li in the singlet state (*b*). The dashed lines depict the deuteron wave function squared.

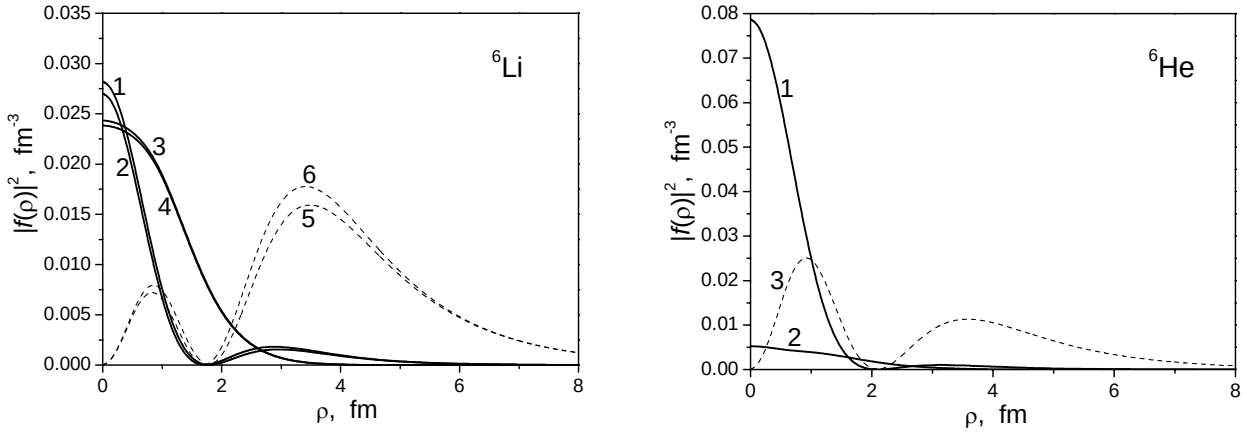

a *b*

Fig. 6. The amplitudes of clusterization (squared) for ^{6}Li. Curve *1* shows $\left|f_{^6Li,\,d}(\rho)\right|^2$; curve *2* - $\left|f_{^6Li,\,d-cluster}(\rho)\right|^2$; *3* - $\left|f_{^6Li,\,\alpha p-cluster}(\rho)\right|^2$; and *4* - $\left|f_{^6Li,\,\alpha n-cluster}(\rho)\right|^2$ (*a*). The same for ^{6}He, where curve 1 shows $\left|f_{^6He,\,nn-cluster}(\rho)\right|^2$, and curve *2* is for $\left|f_{^6He,\,\alpha n-cluster}(\rho)\right|^2$ (*b*). The dashed lines depict $\rho^2\left|f(\rho)\right|^2$, with the correspondence 1↔5, 2↔6 (in Fig. 6, *a*) and 1↔3 (in Fig. 6, *b*).

The deuteron wave function squared is close to the correlation function $g_{np}(r)$ (the latter has, of course, a somewhat smaller radius), and this is valid not only for ^{6}Li nucleus (see, e.g., the calculations for three- and four-nucleon nuclei [9, 10]). Thus, we can consider the modified value $f_{^6Li,\,d-cluster}(\rho)$ similar to (19), but with $\sqrt{g_{np}(r)}$ instead of $\varphi_d(r)$. Then the value of $\left|f_{^6Li,\,d-cluster}(\rho)\right|^2$ is to be the "deuteron cluster" coefficient of clusterization. Its profile (see Fig. 6, *a*, curve *2*, and dashed line *6* – for $\rho^2\left|f_{^6Li,\,d-cluster}(\rho)\right|^2$) is seen to be close to

$\left|f_{^6Li,\,d}(\rho)\right|^2$. The corresponding modified coefficient $C^{(^6Li)}_{d-cluster}$ is defined by a relation similar to (20), and it is equal to 0.75 (0.08 due to the "cigar" configuration, and 0.67 comes from the "triangle").

The modified coefficients of clusterization $f_{^6He,\,nn-cluster}(\rho)$ enable one to estimate the probability for the dineutron cluster to exist in ^{6}He nucleus, although a free dineutron does not exist. In Fig. 6, *b*, we present the dineutron cluster coefficient $\left|f_{^6He,\,nn-cluster}(\rho)\right|^2$. We find the coefficient $C^{(^6He)}_{nn-cluster} = 0.73$ (the first peak in Fig. 6, *b* results in 0.32, and the second one gives 0.41). It is natural that the "cigar" configuration plays a somewhat greater role in ^{6}He than that in ^{6}Li, because the *np* subsystem in the ^{6}Li halo prefers to be a dineutron cluster due to V_{np} in the triplet state is more attractive than V_{nn} in the singlet state. We can also estimate the probability for a five-nucleon cluster (αN-cluster in the $S_{1/2}$ state) to exist inside a ^{6}Li nucleus, by using the modified coefficients of clusterization. The curves for $\left|f_{^6Li,\,\alpha p-cluster}(\rho)\right|^2$ and $\left|f_{^6Li,\,\alpha n-cluster}(\rho)\right|^2$ almost coincide. We obtain $C^{(^6Li)}_{\alpha p-cluster} \approx C^{(^6Li)}_{\alpha n-cluster} \approx 0.60$ for ^{6}Li nucleus. For ^{6}He nucleus, the calculation results in $C^{(^6He)}_{\alpha n-cluster} \approx 0.21$.

The analysis of the asymptotics of amplitude (19) at large ρ enables us to estimate the constant of asymptotic normalization for the process $^6\mathrm{Li} \to \alpha + d$, and this gives directly the corresponding nuclear vertex constant [21, 22]. The asymptotics of (19) is known to be

$$f_{^6Li,\,d}(\rho) \underset{\rho\to\infty}{\to} C_A \rho^{-1} W_{-\eta,\,\frac{1}{2}}(2\kappa\rho) \underset{\rho\to\infty}{\to} C_A\, \rho^{-1} \exp\left(-\kappa\rho - \eta \ln(2\kappa\rho)\right), \qquad (21)$$

where $\kappa = \left(\dfrac{2\left(\left|E_{^6Li}\right| - \varepsilon_d\right)\mu_{\alpha d}}{\hbar^2}\right)^{\frac{1}{2}}$, $\eta = \dfrac{\mu_{\alpha d} Ze^2}{\hbar^2 \kappa}$, $\mu_{\alpha d} = \dfrac{\mu_\alpha \mu_d}{\mu_\alpha + \mu_d}$, and $W_{-\eta,\,\frac{1}{2}}(r)$ is the Whittaker function. Comparing the results of our calculation of $f_{^6Li,\,d}(\rho)$ (reliable up to $\rho \sim 15$ fm, if about 300 Gaussian functions of the basis are used) with the asymptotics (21) (coming into force already at ~6 fm), we have $C_A = 0.693$ fm$^{-1/2}$ and $\sqrt{4\pi}\, C_A = 2.46$ fm$^{-1/2}$ for potential (***I***), and $C_A = 0.705$ fm$^{-1/2}$ and $\sqrt{4\pi}\, C_A = 2.50$ fm$^{-1/2}$ for potential (***II***) from Table 2. The estimate is seen to depend a little on the model of $N\alpha$-interaction, and this is consistent with other calculations [2, 22].

Consider the momentum distribution of particles. For the *j*-th particle, it is given by

$$n_j(k) = \left\langle \tilde{\Phi} \right| \delta\left(\mathbf{k} - \left(\mathbf{k}_j - \mathbf{K}_{c.m.}\right)\right) \left| \tilde{\Phi} \right\rangle, \qquad (22)$$

where $\left|\tilde{\Phi}\right\rangle$ is the momentum representation of the wave function of the system. The average kinetic energy of a neutron in the halo of ^{6}He [7] appears to be $\left\langle E_{kin}\right\rangle_n = 11.12$ MeV, and that of the α-particle is $\left\langle E_{kin}\right\rangle_\alpha = 5.935$ MeV. The average kinetic energies of the proton and neutron in the halo of ^{6}Li are $\left\langle E_{kin}\right\rangle_p = 12.56$ MeV and $\left\langle E_{kin}\right\rangle_n = 12.77$ MeV, respectively, and that of the α-particle is $\left\langle E_{kin}\right\rangle_\alpha = 3.23$ MeV. The momentum distributions are depicted in Fig. 7. The change of regimes in the neutron halo momentum distribution is explained by the fact [23] that the asymptotics at $k \to \infty$ is proportional to $n_n(k) \sim \left(\dfrac{V_m(k)}{k^2}\right)^2$ and reflects the short-range repulsion present in the V_{NN} potentials. Simpler models of potentials without short-range repulsion give no "tail" in $n_n(k)$. The same regularities are observed for $n_n(k)$ in calculations of other authors [24]. The momentum distribution of the neutron $n_n(k)$ in the ^{6}Li halo (Fig. 7, *a*) is very close to that of the proton, $n_p(k)$, which is not shown.

The momentum distribution of the α-particle center of mass is depicted in Fig. 7, *b*. Two regimes in the behavior of $n_\alpha(k)$ are explained, to a great extent, by the presence of two configurations (the "cigar" and "triangle") in the wave functions of the nuclei with $A = 6$ (the former makes the main contribution at high k^2, and the latter does at low k^2). Since the "triangle" configuration in ^{6}Li is more pronounced, and the "cigar" is less probable as compared to that in ^{6}He, the momentum distribution $n_\alpha(k)$ at high k^2 is positioned lower for ^{6}Li than that for ^{6}He.

In the singlet state of ^{6}Li nucleus, the momentum distributions of the proton $n_p(k)$ and the neutron $n_n(k)$ of the halo are also close to each other and surely manifest greater role of small momenta and the less presence of large ones in comparison with

those of $n_n(k)$ for ^{6}He due to the fact that, in the singlet state, ^{6}Li has a less binding energy and a greater size of the halo than ^{6}He nucleus does. The same reason is responsible for the $n_\alpha(k)$ profile behavior for the singlet state of ^{6}Li in comparison with that for ^{6}He. It should be noted that, though the ground state of ^{6}Li has a greater binding energy than ^{6}He does, the momentum distribution $n_\alpha(k)$ of the α-particle center-of-mass of ^{6}Li in the ground state is also positioned lower than $n_\alpha(k)$ for ^{6}He at large momenta and, *vice versa*, higher at small ones (see Fig. 7, *b*), but the reason for this is the suppressed "sigar" configuration in the ^{6}Li ground state (due to the bound deuteron cluster).

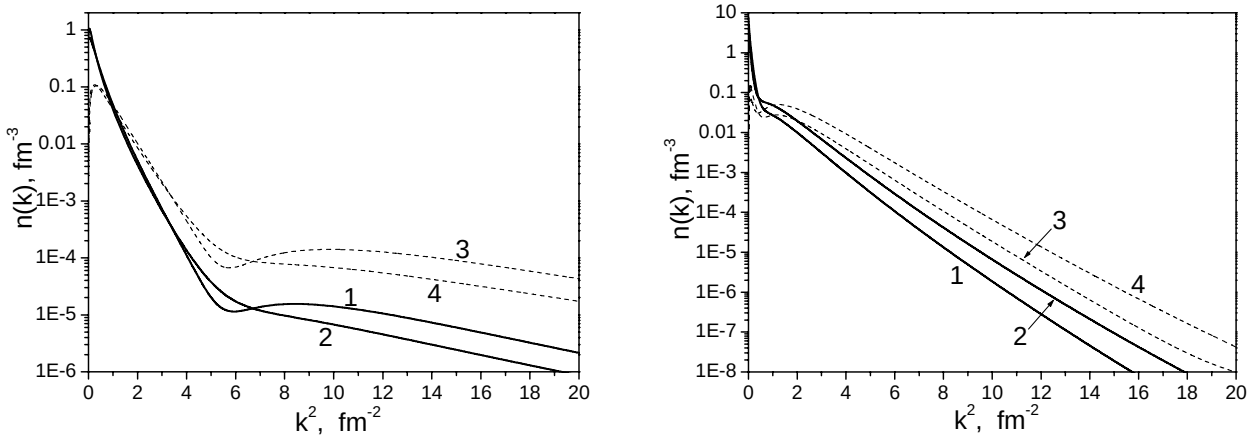

a *b*

Fig. 7. The momentum distributions of a halo neutron in ^{6}Li (curve *1*) and ^{6}He (curve *2*) (*a*). The momentum distribution of the α-cluster in the same nuclei (curve *1* - ^{6}Li, and curve *2* - ^{6}He) (*b*). In both figures (*a*) and (*b*), the dashed lines depict $k^2n(k)$ (curve *3* - for ^{6}Li, and curve *4* - for ^{6}He).

To summerize, we note that the three-particle model for halo nucleus ^{6}Li, as well as for ^{6}He [7], manifests a rather high accuracy. The proposed *Nα*-potentials are fitted so that to reproduce the phase shifts simultaneously with the energy and the radius of a nucleus, and the main structure functions of the nucleus are found and analysed. A nonsingular method to find the phase shifts for the potentials with local and non-local operator terms and with additional Coulomb interaction is proposed.

REFERENCES

1. *Zhukov M. V., Danilin B. V., Fedorov D. V. et al.* Bound State Properties of Borromean Halo Nuclei: ^{6}He and ^{11}Li // Physics Reports. - 1993. - Vol. 231, No. 4. - P. 151 - 199.
2. *Kukulin V. I., Pomerantsev V. N., Razikov Kh. D. et al.* Detailed Study of the Cluster Structure of Light Nuclei in a Three-Body Model (IV). Large Space Calculation for *A* = 6 Nuclei with Realistic Nuclear Forces // Nuclear Physics. - 1995. - Vol. A 586, No. 1. - P. 151 - 189.
3. *Nielsen E., Fedorov D. V., Jensen A. S., Garrido E.* The Three-Body Problem with Short-Range Interactions // Physics Reports. - 2001. - Vol. 347, No. 5. - P. 373 - 459.
4. *Василевский В. С., Нестеров А. В., Арикс Ф., Ван Лёувен П.* Трехкластерный вариант алгебраической версии метода резонирующих групп и его применение к исследованию свойств связанных состояний ядер ^{6}He и ^{8}He // Зб. наук. праць Ін-ту ядерних досл. - 2002. - № 2(8). - С. 51 - 59.
5. *Вербицкий В. П., Поздняков Ю. А., Теренецкий К. О.* Вариационный расчет энергии основного состояния ядра ^{6}He в трехкластерном приближении метода резонирующих групп // Изв. РАН. Сер. физ. - 1996. - Т. 60, № 1. - С. 52 - 57.
6. *Сименог И. В., Ситниченко А. И.* Структура состояний ядер с A = 6 в модели α-(2*N*)-кластеров // УФЖ. - 1978. - Т. 23, № 12. - С. 2052 - 2060.
7. *Гринюк Б. Е., Сименог И. В.* Структура ядра ^{6}He в трехчастичной модели // Ядерная физика. - 2009. - Т. 72, № 1. - С. 10 - 24; *Grinyuk B. E., Simenog I. V.* Structure of the ^{6}He Nucleus in the Three-Particle Model // Phys. Atomic Nuclei. - 2009. - Vol. 72, No. 1. - P. 6 - 19).
8. *Grinyuk B. E., Simenog I. V.* Structure of ^{6}He and ^{6}Li Nuclei within a Three-Particle Model // Proc. of the 2nd Int. Conf. "Current Problems in Nuclear Physics and Atomic Energy" (Kyiv, Ukraine, June 9 - 15, 2008). - Part I. - Kyiv, 2009. - P. 101 - 107.
9. *Grinyuk B. E., Piatnytskyi D. V., Simenog I. V.* Structure Characteristics of a ^{4}He Nucleus within the Microscopic Approach // Ukr. J. Phys. - 2007. - Vol. 52, No. 5. - P. 424 - 435.
10. *П'ятницький Д. В., Сименог І. В.* Ядерні потенціали взаємодії для сумісного опису малонуклонних систем і структурні функції тринуклонних ядер //

УФЖ. - 2008. - Т. 53, № 7. - С. 629 - 639.
11. *Кукулин В.И., Неудачин В.Г., Смирнов Ю.Ф.* Взаимодействие составных частиц и принцип Паули // ЭЧАЯ. - 1979. - Т. 10, вып. 6. - С. 1236 - 1293.
12. *Yao W.-M., Amsler C., Asner D. et al.* Review of Particle Physics // J. Phys. G 33. - 2006. - P. 1 - 1232.
13. *Calogero F.* Variable Phase Approach to Potential Scattering. - N.-Y. and London: Academic Press, 1967.
14. *Бабиков В. В.* Метод фазовых функций в квантовой механике. - М.: Наука, 1976. - 288 с.
15. *Kukulin V. I. and Krasnopol'sky V. M.* A Stochastic Variational Method for Few-Body Systems // J. Phys. G: Nucl. Phys. - 1977. - Vol. 3, No. 6. - P. 795 - 811.
16. *Колесников Н. Н., Тарасов В. И.* Феноменологический *NN*-потенциал из анализа трех- и четырехчастичных ядер // Ядерная физика. - 1982. - Т. 35, вып. 3. - С. 609 - 619.
17. *Audi G., Wapstra A. H.* The 1995 Update to the Atomic Mass Evaluation // Nucl. Phys. - 1995. - Vol. A 595, No. 4. - P. 409 - 480.
18. *De Vries H., De Jager C.W., De Vries C.* // At. Data Nucl. Data Tables. - 1987. - Vol. 36. - P. 495 - 536.
19. *Egelhof P.*, *Alkhazov G. D., Andronenko M. N. et al.* Nuclear-matter distributions of halo nuclei from elastic proton scattering in inverse kinematics // The European Physical Journal. - 2002. - Vol. A 15, No. 1 - 2. - P. 27 - 33.
20. *Filippov G. F., Ovcharenko V. I., Simenog I. V.* Cluster Structure of the Three-Particle Bound State. - Kiev, 1971. - 46 p. - (Preprint / ITP-71-74E).
21. *Блохинцев Л. Д., Борбей И., Долинский Э. И.* Ядерные вершинные константы // ЭЧАЯ. - 1977. - Т. 8, вып. 6. - С. 1189 - 1245.
22. *Блохинцев Л. Д., Игамов С. Б., Нишонов М. М., Ярмухамедов Р.* Расчет ядерной вершинной константы (асимптотического нормировочного коэффициента) для виртуального распада ^{6}Li → α + d в модели трех тел и ее применение для описания астрофизической ядерной реакции d(α, γ)^{6}Li при сверхнизких энергиях // Ядерная физика. - 2006. - Т. 69, № 3. - С. 456 - 466.
23. *Amado R. D., Woloshyn R. M.* Momentum Distributions in the Nucleus // Phys. Lett. - 1976. - Vol. 62 B, No. 3. - P. 253 - 255.
24. *Horiuchi W., Suzuki Y.* Momentum Distribution and Correlation of Two-Nucleon Relative Motion in ^{6}He and ^{6}Li // Phys. Rev. - 2007. - Vol. C 76. - P. 024311-1 – 024311-13.

ТРИЧАСТИНКОВА СТРУКТУРА ГАЛО-ЯДРА ^{6}Li

Б. Є. Гринюк, І. В. Сименог

У тричастинковій моделі ядра ^{6}Li (*α*-кластер і два нуклони гало – *p* та *n*) досліджено структурні властивості системи на основі прецизійного варіаційного методу з гауссоїдним базисом. Вивчено основний триплетний ($J^\pi = 1^+$) і збуджений синглетний ($J^\pi = 0^+$) стани ^{6}Li. Запропоновано потенціали *np*- та *Nα*-взаємодій, що описують *S*-фазу пружного розсіяння при низьких енергіях одночасно з енергією і зарядовим радіусом ядра ^{6}Li. Досліджено розподіли густини, формфактор, парні кореляційні функції, коефіцієнти кластеризації та імпульсні розподіли.

ТРЕХЧАСТИЧНАЯ СТРУКТУРА ГАЛО-ЯДРА ^{6}Li

Б. Е. Гринюк, И. В. Сименог

В трехчастичной модели ядра ^{6}Li (*α*-кластер и два нуклона гало – *p* и *n*) исследованы структурные свойства системы на основе прецизионного вариационного метода с гауссоидальным базисом. Изучены основное триплетное ($J^\pi = 1^+$) и возбужденное синглетное ($J^\pi = 0^+$) состояния ^{6}Li. Предложены потенциалы *np*- и *Nα*-взаимодействий, которые описывают *S*-фазу упругого рассеяния при низких энергиях одновременно с энергией и зарядовым радиусом ядра ^{6}Li. Исследованы распределения плотности, формфактор, парные корреляционные функции, коэффициенты кластеризации и импульсные распределения.

Received 19.12.08,
revised - 11.03.09.